EMG-Torque Dynamics Change With Contraction Bandwidth

Mahsa A. Golkar, *Student Member, IEEE*, Kian Jalaleddini, *Member, IEEE*, and Robert E. Kearney, *Fellow, IEEE*

***Abstract*— An accurate model for ElectroMyoGram (EMG)-torque dynamics has many uses. One of its applications which has gained high attention among researchers is its use, in estimating the muscle contraction level for the efficient control of prosthesis. In this paper, the dynamic relationship between the surface EMG and torque during isometric contractions at the human ankle was studied using system identification techniques. Subjects voluntarily modulated their ankle torque in dorsiflexion direction, by activating their tibialis anterior muscle, while tracking a pseudo-random binary sequence in a torque matching task. The effects of contraction bandwidth, described by torque spectrum, on EMG-torque dynamics were evaluated by varying the visual command switching time. Nonparametric *impulse response functions* (IRF) were estimated between the processed surface EMG and torque. It was demonstrated that: 1) at low contraction bandwidths, the identified IRFs had unphysiological anticipatory (i.e., non-causal) components, whose amplitude decreased as the contraction bandwidth increased. We hypothesized that this non-causal behavior arose, because the EMG input contained a component due to feedback from the output torque, i.e., it was recorded from within a closed-loop. Vision was not the feedback source since the non-causal behavior persisted when visual feedback was removed. Repeating the identification using a nonparametric closed-loop identification algorithm yielded causal IRFs at all bandwidths, supporting this hypothesis. 2) EMG-torque dynamics became faster and the bandwidth of system increased as contraction modulation rate increased. Thus, accurate prediction of torque from EMG signals must take into account the contraction bandwidth sensitivity of this system.**

***Index Terms*— Contraction dynamics, EMG-force dynamics, closed-loop system, system identification, tibialis anterior muscle, feedback control.**

Manuscript received January 24, 2017; revised June 21, 2017 and December 18, 2017; accepted January 30, 2018. Date of publication February 16, 2018; date of current version April 6, 2018. This work was supported by NPRP from the Qatar National Research Fund (a member of the Qatar Foundation) under Grant 6-463-2-189. The statements made herein are solely the responsibility of the authors. The work of M. A. Golkar was supported by a Doctoral Scholarship from the Fonds de Recherche du Québec–Nature et Technologies. *(Corresponding author: Mahsa A. Golkar.)*

M. A. Golkar and R. E. Kearney are with the Department of Biomedical Engineering, McGill University, Montréal, QC H3A 2B4, Canada (e-mail: mahsa.aliakbargolkar@mail.mcgill.ca; robert.kearney@mcgill.ca).

K. Jalaleddini is with the Division of Biokinesiology and Physical Therapy, University of Southern California, Los Angeles, CA 90089 USA (e-mail: seyed.jalaleddini@mail.mcgill.ca).

Digital Object Identifier 10.1109/TNSRE.2018.2805472

I. Introduction

THE surface ElectroMyoGram (EMG) provides a convenient, non-invasive measure of the neural activation of a muscle. Surface EMG has many uses: in clinics as a diagnostic tool [1]–[3]; in rehabilitation as a control signal for prosthetic or assistive devices [4]–[7]; and in research to understand the neural control of movement and posture control [8], [9]. All these applications assume, either explicitly or implicitly, that there is a direct relation between surface EMG and muscle force. Consequently, it is important to have accurate models of this relation in functionally significant tasks.

Under stationary or quasi-stationary conditions, it is well documented that there is a monotonically increasing relationship between the EMG intensity (e.g. the mean absolute, average absolute (low-pass filter), sum absolute (integral of absolute) or root mean square) and the measured force or torque [10]–[12]. Under dynamic conditions, where force changes rapidly with time, the EMG-force (torque) relationship has been studied, using two main approaches.

The first approach uses *a priori* models with a fixed structure and parameter values based on prior information (e.g., Hill-type models as the most popular choice) [13]–[15]. This approach is widely used, however, this is mainly based on in-vitro, animal studies, and the model parameters are not straightforward to customize to every subject.

The second approach uses *data-driven models* to estimate the model structure and parameters directly from experimental data. This approach estimates models that best describe the data for each task and will be more accurate than a-priori models for example, for tasks which span wider range of contractions where EMG-torque dynamics are expected to be nonlinear [16]. A number of studies used this technique to estimate EMG-force dynamics during isometric contractions [16]–[26]. However, these studies all used high bandwidth contractions. In practice, most functional tasks involve lower contraction bandwidths. Motor control theory suggests that the motor units are recruited according to size principle and the larger units have faster responses. Consequently, it is reasonable to expect EMG-torque dynamics to change with contraction bandwidth. The effect of contraction bandwidths on EMG-torque dynamics have never been studied.

This paper revisits the surface EMG-torque system, aiming to explore the effect of contraction frequency content on

TABLE I
SUBJECT CHARACTERISTICS: GENDER, AGE AND *MAXIMUM VOLUNTARY CONTRACTION* (MVC) TORQUE IN DORSIFLEXION DIRECTION

Subject	Gender	Age (years)	MVC (Nm)
S1	M	27	39.3
S2	M	31	51.6
S3	M	31	22.9
S4	M	25	31.5
S5	F	26	21.8
S6	M	30	49.4

system dynamics. We used a non-parametric system identification approach to investigate the effect of contraction bandwidths on EMG-torque dynamics of *Tibialis Anterior*. Some preliminary results of this work have been presented at a conference [27].

II. METHODS

A. Subject

Six subjects with no history of neuromuscular disease participated in this study after giving informed consent to the experimental procedures, which had been reviewed and approved by McGill University Institutional Review Board. Table I summarizes the subjects' demographics.

B. Apparatus

Figure 1 shows a schematic of the experimental setup. Subjects lay supine with their left foot attached firmly to the pedal of a servo-controlled hydraulic actuator using a custom-made fiberglass boot [28]. The subject's knee was immobilized in a fully extended position using sandbags and a knee strap. Ankle position was measured using a potentiometer (Beckman 6273-R5 K), and torque measured with a very stiff (50kNm/rad) torque transducer (Lebow 2110-5K). The hydraulic actuator was controlled using an xPC-Target machine programmed to operate as a position servo that maintained the angle between the foot and shank at 90 degrees. Torque and EMG data were filtered with an anti-aliasing filter at 486.3 Hz, sampled at 1 kHz, and recorded with 24 bits resolution using NI-4472 A/D cards.

C. EMGs

EMG signals from *Tibialis Anterior* (TA) and *Triceps Surae* (TS) including Soleus, Medial and Lateral Gastrocnemius, were recorded using differential Bagnoli Delsys surface electrodes. The EMG electrodes were placed according to the SENIAM recommendations [29]: the electrodes were placed at 1/3 on the line between the tip of the fibula and the tip of the medial malleolus for TA muscle, and at 2/3 of the line between the medial condylis of the femur to the medial malleolus for Soleus muscle. A DermaSport reference electrode (American Imex, Irvine) was placed on the subject's patella given its electrically neutral property. This electrode was formulated with an aggressive gel and perforated carbon which helps dissipate moisture and enhance current dispersion. Thus, it has high electrical conductivity and strong adhesive

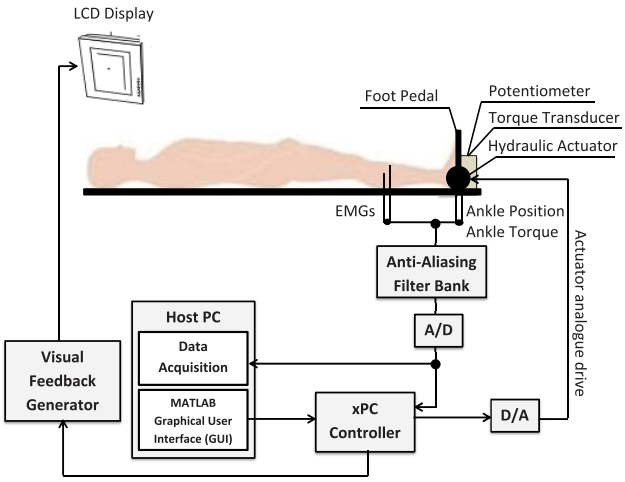

Fig. 1. Schematic of the experimental setup. The subject's left foot was attached to the actuator pedal by a custom boot. Ankle torque and a target signal were displayed on an overhead monitor. The subject generated dynamic, isometric contractions of TA by tracking the target signal.

property. EMGs were amplified with a gain of 1000 and band-pass filtered 20-486.3 Hz [30], [31]. After sampling, EMG signals were full-wave rectified. The resulting signal is referred to as processed EMG from hereinafter.

D. MVCs

The dorsiflexing *Maximum Voluntary Contraction* (MVC) torque of the ankle was measured. Subjects were instructed to maximally contract the ankle dorsiflexor muscles (TA) in response to a sequence of five step changes in visual command. The maximum value of the torque in the five trials was taken as the subject's MVC. Table I gives the MVC for each subject.

Similarly, the *Maximum Voluntary EMG* (MVE) was calculated for EMG signals. The raw EMG was full-wave rectified and filtered with a forth-order low-pass Butterworth filter, with cutoff frequency equal to 1Hz, and the maximum value of the resultant signal was taken as the MVE for the active muscle. MVE for TA and Soleus muscles were calculated from dorsiflexing and plantarflexing MVCs, respectively. The EMG signals were normalized to their MVE for visualization purposes.

E. Trials

All trials were performed in the dorsiflexion direction. Subjects were instructed to use only the TA muscle and not activate the plantarflexor muscles. Two types of quasi-stationary trials were acquired:

1. Visual Feedback (VF): Subjects modulated their ankle torque by tracking a target signal displayed on an overhead monitor. Ankle torque was filtered by an eighth-order, low-pass, Bessel filter with a 0.7 Hz cutoff and fed back to the subject on a monitor. The Bessel filter was only used for visual feedback. *Pseudo Random Binary Sequence* (PRBS) signal was used for visual target. The PRBS signal is a deterministic binary sequence that exhibits statistical behavior similar to a random

sequence and is characterized by its switching time. At the multiples of switching times the signal either switches from one level to another or remains invariant with equal probabilities. The amplitude of the signal is defined by the desired peak-to-peak value. PRBS signals with mean value of 5% MVC and peak-to-peak amplitude of 10% MVC were used. The switching time of the PRBS was selected randomly from $\{0.1, 0.2, 0.3, 0.5, 2, 4\}$ s. One trial was performed at each switching time.

2. No Visual Feedback (NVF): Subjects were instructed to modulate their ankle torque voluntarily in a limited range in absence of visual feedback. Prior to the experiment, subjects were trained to generate the same mean and range of torque as for VF trials. Data was monitored online and trial was repeated if the torque limit (10% MVC) was exceeded. Two sets of trials were performed: one at a slow rate around 0.5 Hz and another at their fastest comfortable rate.

Each trial lasted 60 seconds and a rest period of 2 min was enforced between trials to prevent fatigue.

EMG and torque signals were inspected for evidence of fatigue and/or co-contraction. Moving average estimates of the mean torque signal and standard deviation of the rectified TA EMG were monitored along and across trials. Any systematic change in these was taken as evidence of fatigue; there was no evidence in any of the trials. Soleus EMG was also monitored to ensure there was no agonist-antagonist co-contraction. No co-contraction was found in any trials. The mean values of EMG and torque were removed prior to identification to avoid any bias due to non-physiological offsets in the data record [32], and to benefit from features of linear identification.

Remark: If results are to be used for real-time processing, the estimation of mean value needs to be integrated with the identification algorithm.

F. Identification Algorithm

1) Open-Loop (OL) Identification: An *Impulse Response Function* (IRF) model was estimated between processed EMG and the ankle torque using a pseudo-inverse method [33] that can estimate both one-sided and two-sided filters. This method is based on ordinary least squares and the estimates are best linear unbiased estimates if the noise is independent of the regressor (i.e. data being acquired from an open-loop system). It minimizes the error between the measured and predicted output and thus treats both bias and random errors equally.

2) Closed-Loop (CL) Identification: Preliminary results using the OL identification method showed that estimated IRFs were non-causal supporting the hypothesis that the data were acquired from within a CL system. Consequently, we also used a CL identification method [34] that models the plant as a finite impulse response filter (IRF), and the noise as an autoregressive-moving-average (ARMA) process. Thus, the method identifies the feed-forward pathway in presence of feedback without having to identify the feedback dynamics, if any. The system parameters are estimated using a Separable Least-Squares (SLS) technique that iteratively solves a non-linear least-square optimization problem. The prediction error was defined as the residual of the torque following the subtraction of the predicted torque (from IRF) and passed through inverse of noise model (from ARMA). The IRF length was fixed to 2s based on previous results [16], [21]. The number of zeros/poles of ARMA model was determined empirically by repeating the estimation using different noise models until the prediction error became white, zero-mean, had a Gaussian distribution, and was uncorrelated with the input.

G. Analysis Procedure

1. The quality of the estimated model for each trial was assessed based on how accurately the estimated IRF predicted the measured torque. This was quantified as the percentage of the identification *Variance Accounted For* (%VAF):

$$\%VAF = \left[1 - \frac{\sum_{k=1}^{N}(tq(k) - \hat{tq}(k))^2}{\sum_{k=1}^{N} tq(k)^2}\right] \times 100$$

where, $tq(k)$ and $\hat{tq}(k)$ are the measured and predicted torque at time k and N is the number of data samples. *Remark:* For each trial, the data record was truncated into two sets: 70% was used for identification and the remaining 30% was used for validation. As expected, given that the data record is many times longer than the system memory/parameters (60 versus 2 seconds), the %VAF were very similar. We verified that the differences in identification and validation VAFs were not significant by performing a one-way ANOVA test with significance level equal to 0.05. We chose to present the identification results obtained with full data record in this paper to obtain the most accurate IRFs for our analysis.

2. The torque bandwidth was calculated by finding the cutoff frequency of a moving average filter fitted to the torque signal for each trial. The cutoff frequency was defined to be the frequency where torque power dropped to half of its power at low frequencies (3 dB point).
3. The ratio of power of negative lags to total IRF power was used as *causality index* which ranges from a value of 1 for a purely non-causal IRF to zero for completely causal. The power was calculated as the integral of absolute values of IRF at corresponding lags.

III. Results

A. Experimental Data

Figure 2 shows the normalized torque and EMGs from the dorsiflexing (TA) and plantarflexing (Soleus) muscles for a typical VF trial. The torque signal was normalized to MVC and processed EMGs were normalized to their corresponding MVE, as described in section II-D. Note the absence of any significant activity in the flat Soleus EMG demonstrating that there was no co-contraction. In addition, the intensity of the TA EMG remained constant throughout the experiment indicating that there was no muscle fatigue.

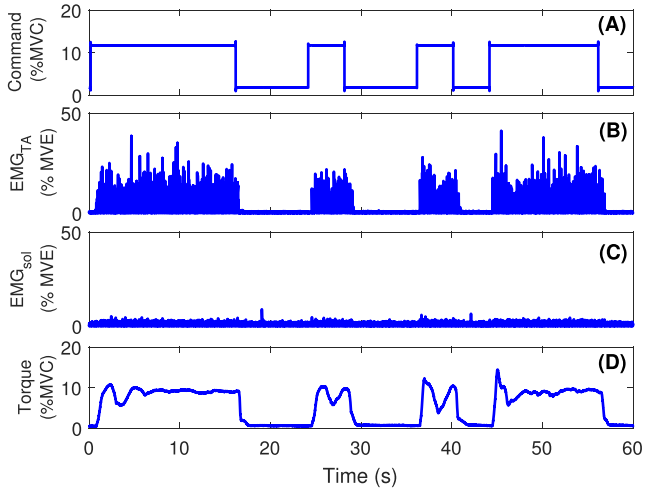

Fig. 2. Typical experimental trial from an isometric contraction experiment. The torque command trajectory was a PRBS with a slow switching time = 4s: (A) command signal, (B) TA EMG, (C) Soleus EMG, (D) ankle torque. Subject S2.

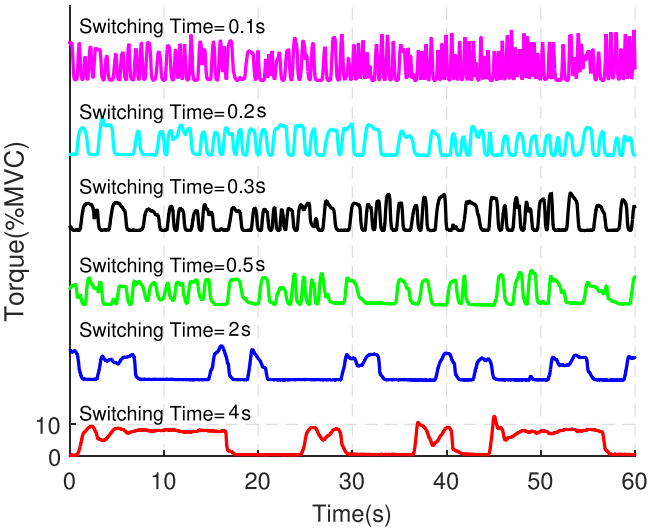

Fig. 3. Typical measured torques for command signals with different switching times. Torques have been displaced upward from one another for clarity. Subject S2.

Figure 3 shows the torque records from a typical subject, tracking commands with different switching times. The subject performed the task successfully in all trials, generating torques with similar means and variances. Figure 4 shows that the torque bandwidth increased as the command switching time decreased.

B. Open-Loop Identification

Figure 5 shows the one and two-sided IRFs estimated from the data shown in Figure 2, using the OL identification technique. The one-sided IRF (blue trace) has a value at zero-lag that is much greater than zero which implies that the torque is generated instantly in response to EMG. This is not consistent with the physiology and mechanics of the activation-contraction dynamics given the low-pass nature of this system; the rate of calcium release and its removal from/to

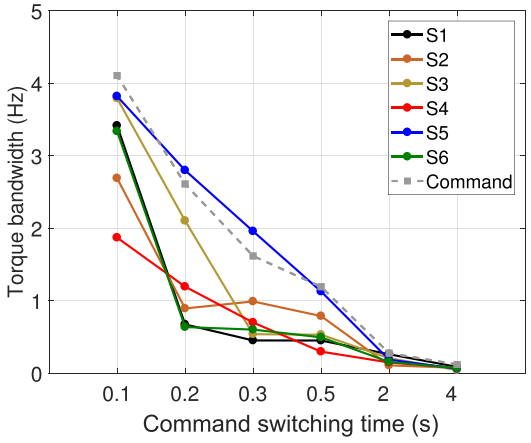

Fig. 4. Torque bandwidth as a function of the command signal switching time.

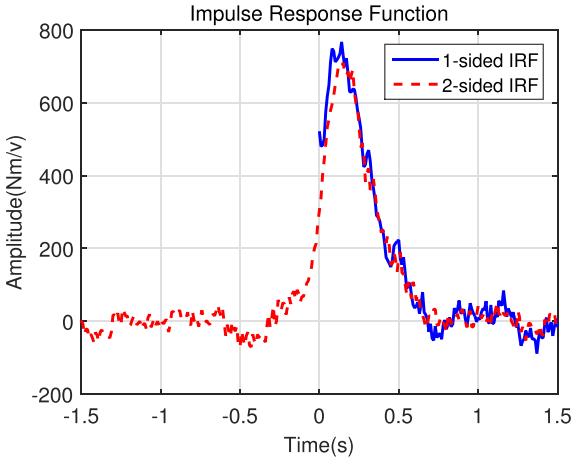

Fig. 5. Identified one-sided and two-sided IRFs relating processed EMG as input to the ankle torque as the output using an open-loop identification technique from the data shown in Figure 2 with switching time equal to 4s. Subject S2.

the sarcoplasmic reticulum result in a sluggish force generation process which does not allow instantaneous generation of force. The 2-sided IRF, the red trace in Figure 5, had values that were significantly different from zero at negative lags, indicating that the system was non-causal. However, as explained above, a physiological system cannot be non-causal but its estimates can be, if an incorrect model is assumed. A similar behavior was observed in all subjects for contractions with this low bandwidth.

Neither the instantaneous force generation of the one-sided filter, nor the anticipatory behavior of the two-sided filter seem physiologically reasonable. Nevertheless, we examined our data to see if either had occurred. To do so, we computed ensemble averages of processed EMG and torque for 5 seconds centered around the activation or deactivation commands for 12 segments. Figure 6 shows a typical pair of ensemble averages which clearly demonstrate that the torque change follows the change in EMG and that there is no evidence of instantaneous or anticipatory force generation. This was only used for visual verification and to examine the

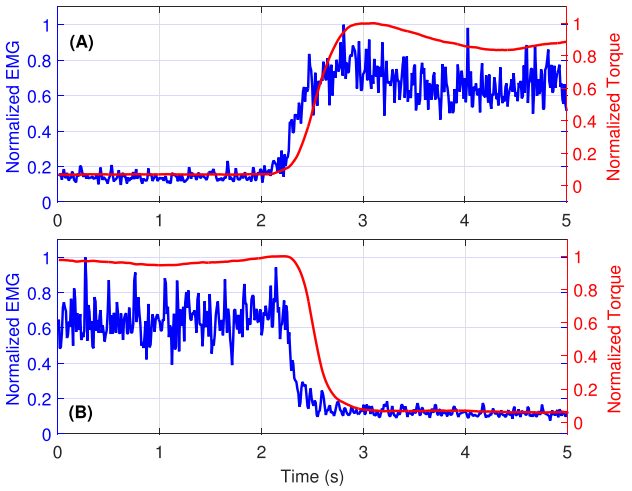

Fig. 6. Ensemble average of EMG and Torque for task with switching time = 4 s, for: (A) activation phase, (B) deactivation phase. The torque change follows that of the EMG. Subject S2.

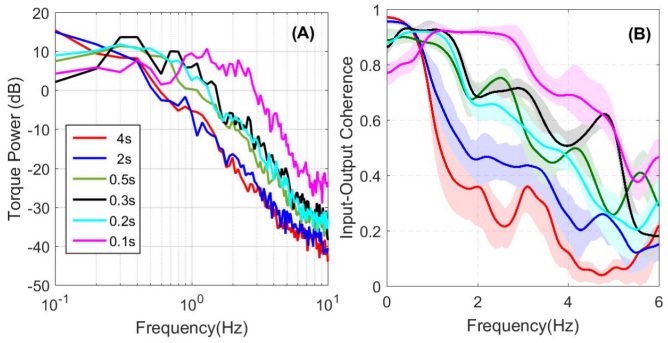

Fig. 7. (A) Power spectrum of torque for different switching rates shows that torque had significant power beyond the cutoff frequency. (B) Coherence between processed EMG and torque shows that low-frequency coherence was high demonstrating reliable estimate of the system dynamics in this frequency range. Subject S2.

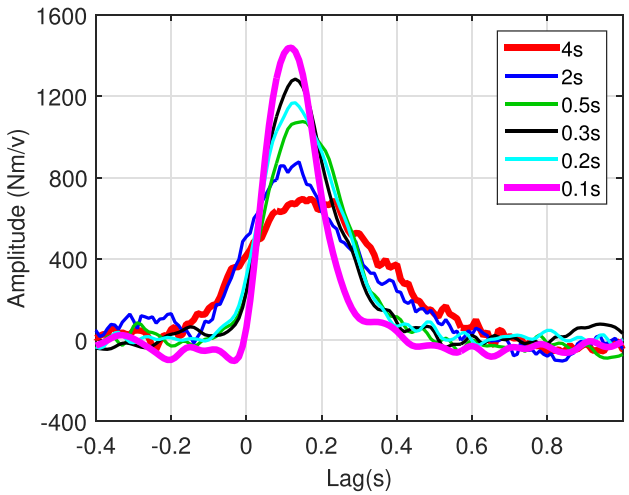

Fig. 8. Two-sided IRFs estimated at different command switching times. Subject S2.

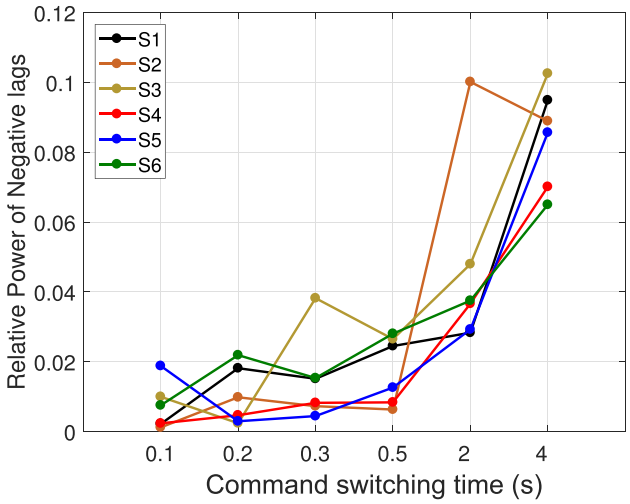

Fig. 9. Causality Index: Relative power of normalized IRFs negative lags increases as a function of the switching time of the visual command.

phase lag between the EMG and the torque signals and thus to inspect the causality of the system.

Next, we studied the effect of contraction bandwidth on EMG-torque dynamics by changing the switching time of the command signal. Figure 7A shows the torque power spectra at the different switching rates demonstrating that there was significant power beyond 2Hz in all cases. Moreover, as Figure 7B demonstrates, the coherence between the processed EMG and torque remained substantial at these frequencies as well. These results indicate that the input stimulus was rich enough to permit out identification algorithm to estimate EMG-torque dynamics reliably.

Figure 8 shows the 2-sided IRFs calculated between the processed EMG and measured torque for the trials of Figure 3. The predicted torque followed the measured torque accurately with identification %VAF of 95.83±1.6%. The amplitude of the IRF weights at negative lags decreased as the switching time decreased; the IRF estimated for trial with smallest command switching time became causal.

Figure 9 shows the causality index calculated for each subject. The non-causal behavior decreased as the command switching time decreased, becoming negligible at the 0.1s rate. This behavior was consistent in all six subjects. The identification %VAF was 93.69±1.07% for all subjects and trials.

C. No Visual Feedback

We hypothesized that the anticipatory components in the IRF estimates might be associated with the visual feedback of ankle torque. To test this, we compared the IRFs estimated from data acquired in the VF and NVF conditions. The switching time of the NVF slow contraction trial was close to the trial with the largest switching time in VF experiments. This case had the largest non-causal behavior in VF experiments and was selected to investigate the effect of visual feedback. As Figure 10 illustrates, the IRFs estimated with and without visual feedback had similar anticipatory components. The IRFs estimated from the fastest modulation rate trials had a causal behavior, similar to the VF case. A similar behavior was observed in all subjects examined. Thus, visual feedback cannot be the major source of the non-causal IRF estimated.

D. Closed-Loop Identification

Although visual feedback does not appear to be responsible for the non-causal behavior, feedback from sensory mechanisms remains a possibility. To test this, we repeated the estimation using a CL algorithm that will correct for bias due to feedback.

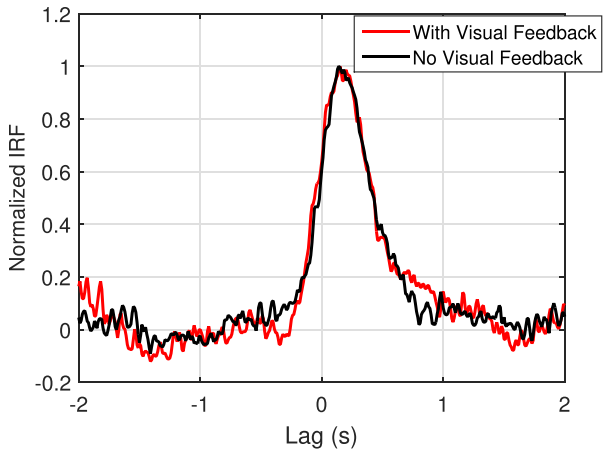

Fig. 10. EMG-Torque normalized IRFs estimated from experiments with and without visual feedback, Subject S2. The torque bandwidth was around 0.5 Hz.

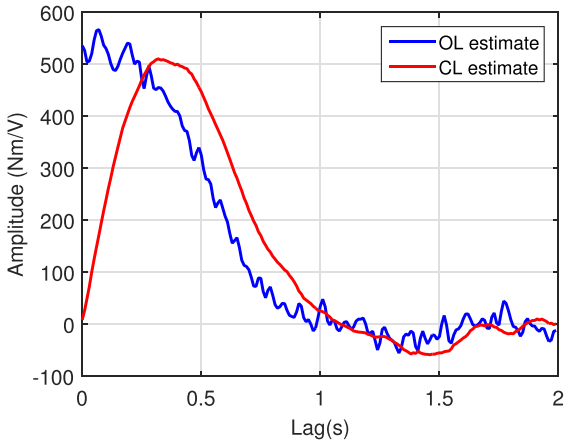

Fig. 11. IRF identified using the open-loop and closed-loop identification techniques for command switching time 4s. Subject S2.

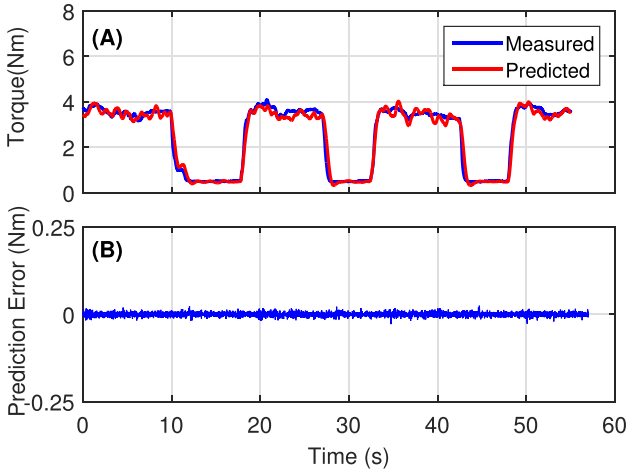

Fig. 12. Prediction performance for estimated model in Figure 11 using the CL identification method: (A) Observed and predicted torque, (B) Prediction error calculated as the difference between the measured and predicted torques, when the effect of estimated noise dynamics is removed. Subject S2.

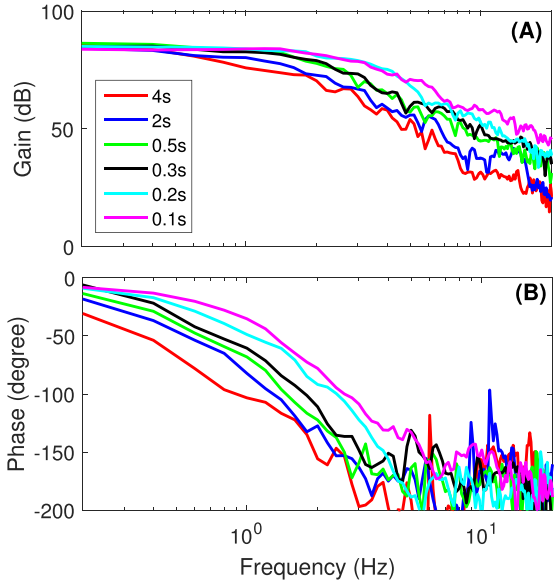

Fig. 13. Frequency response of the IRFs estimated using CL method for trials of Figure 3. The system bandwidth increased as the contraction bandwidth increased. Subject S2.

Using the model selection criteria described in section II-F.2, a 2 seconds long IRF and an ARMA model with 1 zero and 16 poles were selected to describe the plant dynamics and noise model, respectively. Figure 11 shows the 1-sided IRFs estimated with the OL and CL methods for a typical trial. The OL represented a non-causal system. The CL IRF was zero at zero-lag indicative of a causal system. Figure 12A shows the predicted torque followed the measured torque accurately. The identification %VAF for this experiment was %92.2 and the residuals were small as demonstrated in Figure 12B. The %VAF was 92.18±1.82% for all trials acquired from 6 subjects.

Figure 13 shows the frequency response of the IRFs estimated using CL method for trials of Figure 3. The bandwidth of system increased with contraction bandwidth. The bode diagram of the system dynamics is consistent with that of second-order low-pass filter.

IV. Discussion

This work studied the dynamic relationship between EMG and torque in human ankle for isometric contraction tasks. Our results showed that: 1) IRFs estimated using OL method had non-causal components which are not physiologically possible; 2) The non-causal component were consistent with the existence of feedback pathways as verified by applying a CL identification algorithm, and so CL identification methods are necessary to get unbiased estimate of EMG-torque dynamics; 3) The anticipatory component of OL IRFs became progressively smaller as the contraction bandwidth increased, suggesting that if the CL hypothesis is proven correct, the feedback contribution became minimum at high contraction bandwidths; 4) The system relating processed EMG to torque (shown to have second-order low-pass filter dynamics [27]) became faster as the contraction bandwidth increased. Each of these findings will be discussed in detail in subsequent sections.

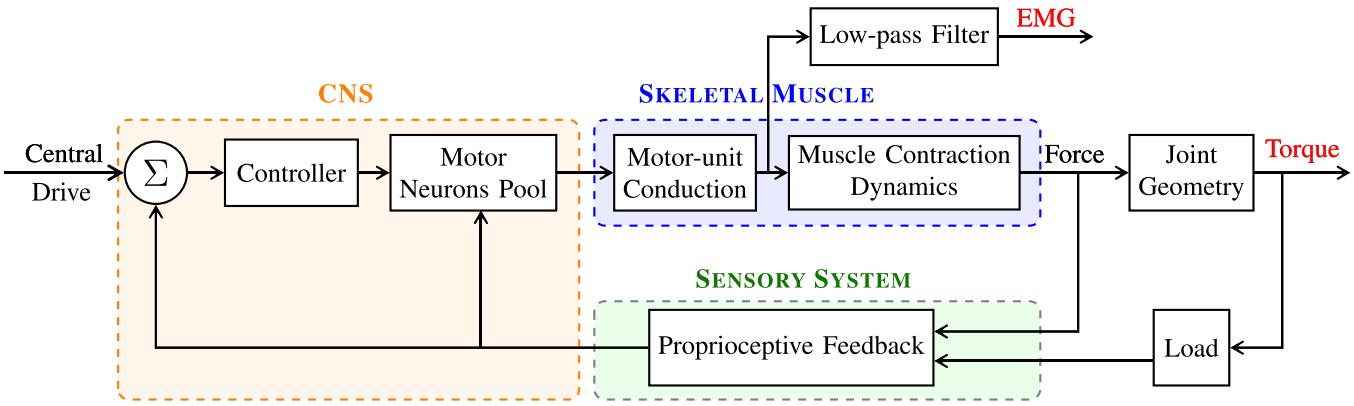

Fig. 14. Expected model for skeletal muscle force generation mechanism. The proprioceptive feedback in force production task provides information about muscle force, muscle length and its rate of change. The low-pass filter block in generating the EMG signal models the spatial filter behavior of the muscle fibers, subcutaneous fat and skin tissues.

A. EMG-Torque Dynamics: Part of a Closed-Loop System

We examined the dynamic relationship between processed EMG and torque using system identification methods. Our results showed that the IRFs identified for low-bandwidth contraction trials had non-physiological anticipatory component. This is known to appear when data is recorded from inside a CL system [35], [36].

From the literature we know that there are many candidates for feedback in the human force generation mechanism. Chief among them are the proprioceptive feedback (i.e. Golgi tendon organ and muscle spindle). Figure 14 represents the expected force generation mechanism in human skeletal muscle. The neural input to muscle (output of motor unit conduction block), recorded as EMG signal, results from alpha-motorneuron activation which receives feedback from sensory receptors through afferent nerves. The voluntary muscle contraction gives rise to input that in turn alters the central drive. Thus, the EMG signal is driven by both the central drive and feedback and so is recorded from within a closed-loop. The results obtained using the nonparameteric, CL-based identification algorithm is in line with this discussion. The CL identification algorithm, which is designed specifically to eliminate bias due to feedback, always produced IRF estimates with only causal behavior.

Note that we wish to identify the OL EMG-torque dynamics. However, if these dynamics are embedded within a closed-loop system, as illustrated in Figure 14, open-loop identification methods will yield biased estimates including anticipatory components. Such biased estimated models may predict the CL output well even though they do not reflect the underlying OL dynamics. CL identification methods must be used to identify this OL model encompassed in a CL structure accurately. The CL identification algorithm used in this work, does not estimate the full closed-loop model.

Different mechanism can contribute to the feedback system including proprioceptors or skin receptors. For instance, muscle afferents are known to have both central and peripheral interactions and can regulate the descending command to facilitate task execution [37]–[43]. Since we do not have access to the internal signals, we cannot identify the actual source of the feedback, however we ruled out visual feedback by repeating the experiments blindfolding the subjects. We also verified that the input frequency content did not affect our results by running a simulation study using our experimentally recorded input signal (see Appendix). Nevertheless, the hypothesis that the data were recorded from within a CL system is a sufficient condition to explain the observed non-causal behavior. However, the fact that our results were consistent with CL system and that the identified models described the observed behavior well, do not guarantee that this is the reason for the non-casual behavior as we have not identified the source of the feedback.

If the internal signals from central drive can be accessed and recorded (e.g., using invasive approaches), one can fully establish the underlying dynamics of the CL behavior. This would be beneficial to explain which pathway is responsible for the observed behavior. Moreover, investigating the CL system bandwidth may also provide insight into the role of feedback in the overall force generation mechanism in terms of system response time.

B. Implications for Understanding Motor Control

Our results showed that the anticipatory component of the estimated IRFs decreased as the contraction bandwidth increased. We demonstrated that the underlying dynamics were consistent with the data being acquired from within a CL system when the contraction bandwidth was small. In the context of a CL system, these results suggest that the contribution of the feedback progressively decreased with increase in contraction bandwidth. System became OL for the highest contraction bandwidth tested. We attribute this as a shift from a feedback to feedforward (pre-programmed) control strategy.

This hypothesis is consistent with former *movement* planning studies which suggest that in slow movements, a feedback control strategy is primarily used which relies on sensory signals to correct the movement whereas in ballistic movements a feedforward strategy is used which does not rely on sensory feedback [44]. This is presumably because in ballistic

contractions, the task need to be accomplished very fast and the sensory signals lose their utility mainly because of their inherent delays [45], [46]. Other possibility is that as the contraction switching rate increases, subjects progressively pay less attention to their force trajectory and shift to a rhythm control strategy which is essentially feedforward [47]. The motor control theories also support a shift to feedforward strategies to generate rapid reaching movements [48], [49]. Previous studies revealed that spinal reflexes modulate in a task-dependent manner in leg muscles [50]–[52] and hand muscle [53] to adapt to the task requirements. This has been interpreted as evidence of dynamic change and the role of proprioceptive feedback for optimal performance and control of limb movement [53]. We interpret our results as demonstrating the role of significant non-visual feedback components in the control of low-bandwidth contractions.

Some other possibility of observed decrease in feedback contribution with contraction bandwidth, are the unresponsive behavior of feedback mechanism to high contraction input (torque generated in high contraction bandwidth tasks) or modulation in feedback gain (presynaptic inhibition) through Central Nervous System (CNS) with increase in torque bandwidth.

C. Contraction Bandwidth Sensitivity

We studied the dependence of EMG-torque on contraction bandwidth by calculating the frequency response of the IRFs estimated from CL method. Our results revealed that system bandwidth increased with contraction frequency content (Figure 13).

The observed behavior was not due to the low bandwidth input power at low switching rate contractions. Our coherence plot confirmed that the input-output signals were coherent beyond the torque cutoff frequency (Figure 7). Furthermore, a simulation study demonstrated that our identification algorithm can estimate the dynamics accurately using our experimental inputs (see Appendix). Moreover, in a previous work, we showed that we can accurately identify the dynamics of the highest-bandwidth system using data from the slowest torque-varying experiment [54]. Thus, we believe that changes in EMG-torque dynamics that we report reflect physiological changes rather than estimation problems.

We attribute the faster dynamics to faster motor units; they are typically larger and have a faster response. However, according to the size principle they are recruited later than smaller motor units. Given the low-pass filter behavior of muscle, and the fact that smaller units have a slower response and require longer time to built up the required force, larger motor units need to be recruited during ballistic tasks to maintain the desired force magnitude [45], [55]. Thus, our results suggest that in high switching rate contractions, faster motor units are recruited at a lower contraction level.

Note that, the contraction switching rate was the independent variable in this study. System bandwidth and closed-loop behavior changed with torque switching rate. However, we have no evidence that there is any causal relation between the changes in closed-loop behavior and system bandwidth.

D. Comparison With Previous Work

Previous studies of EMG-force dynamics have not reported a non-causal IRF estimate or CL behavior. This is not surprising for works that used an *a priori* model to represent the dynamics; the alternatives were never explored. The few works who have used system identification, e.g., [16], [21], however, used a visual command signal with very fast contraction switching rate (switching time $<$ 300ms) close to the fastest contractions studied in this work, where we found the contribution of the feedback to be insignificant. In this work, we showed that especially for low bandwidth contractions, a CL method should be used to estimate the EMG-torque dynamics. It should be noted that using an OL approach to model this system may provide a good prediction of torque but the resulting model is not correct and may not be accurate for estimating torque for a different trial.

Some previous studies have demonstrated the need to use filters with time-varying cutoff frequency for EMG amplitude estimation with application in myoelectric control of prosthetics [56]–[60]. The cutoff frequency of filter was either adjusted manually or by using adaptive filtering techniques. The main objective was to adapt to changes in the frequency content of EMG with fatigue. However, they also provided evidence that the filter cutoff frequency needed to be adjusted with respect to task modulation rates, even though they did not study the EMG-torque dynamics explicitly. The cutoff frequency of the resulting filters can be proportional to the EMG-torque dynamics bandwidth. In this work, we provided evidence for the existing correlation between cutoff frequency of such processing filters and generated torque bandwidth and documented the changes in EMG-torque dynamics with contraction bandwidth.

V. Conclusions

An accurate, custom-made, comprehensive model for muscle EMG-force (or torque) is essential to understand motor control and for the design of efficient assistive devices. This paper demonstrated the need to use CL method to study the EMG-torque dynamics and its necessity to acquire an accurate, unbiased estimate of the dynamics of this system when system identification is used especially when contraction bandwidth is below 2Hz. It was also demonstrated that such a model must incorporate the dependence on contraction bandwidth: as torque bandwidth was increased i) the magnitude of feedback decreased and system became open-loop for modulations faster than 2Hz, ii) system bandwidth increased and system became faster. Thus, in designing filters this property needs to be accounted for.

Our results have important implications for any application which uses EMG to predict torque since we provided evidence that the system dynamics is sensitive to contraction bandwidth. Moreover, the change in impulse response function estimates as a function of contraction bandwidth may provide insight into the motor control strategy and the relative contributions of rate coding-recruitment in force generation.

Our results describe the behavior of this system around a particular operating point (fixed muscle-tendon length and

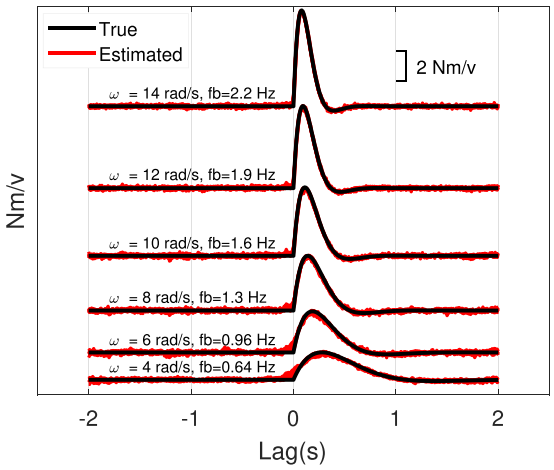

Fig. 15. Two-sided IRFs estimated for simulated linear system with a range of natural frequencies (4-14 rad/s). The simulated and estimated IRFs are displayed upward from one another for clarity. ω is the natural frequency of the simulated system and *fb* is the resulting system bandwidth.

contraction mean) and explain how the EMG-force dynamics behave as a function of contraction bandwidth when the mean contraction level and depth of modulation are constant. More experiments spanning different contraction levels, contraction amplitudes and muscle lengths need to be done and this system needs to be further investigated to acquire a comprehensive model which takes into account the inherent nonlinearities due to the large change in contraction level [16] and joint angle [61], [62]; this is subject of our future work.

APPENDIX

We used a simulation study to demonstrate that the inputs were rich enough to yield reliable estimates for all switching rates. We simulated the responses of a second order low-pass filter system to the experimental EMG recorded for the slowest torque modulation trial (4s switching rate). The filter gain was 1, the damping ratio 0.7, and the natural frequency was varied from 4 to 14 rad/s in 2 rad/s increments. This covered the range of bandwidths identified for this system from experimental data at different contraction bandwidths. Two-sided IRFs were estimated between the experimental EMG input signal and the simulated output signal for each natural frequency. Figure 15 shows the true and estimated IRFs; these were causal and accurate for all filter parameters demonstrating that input had sufficient power to accurately retrieve the system dynamics.

ACKNOWLEDGMENTS

The authors would like to thank Dr. Ross Wagner for his technical assistance with experimental work.

REFERENCES

[1] K. C. McGill, Z. C. Lateva, and H. R. Marateb, "EMGLAB: An interactive EMG decomposition program," *J. Neurosci. Methods*, vol. 149, no. 2, pp. 121–133, 2005.

[2] A. Holobar, M. A. Minetto, A. Botter, F. Negro, and D. Farina, "Experimental analysis of accuracy in the identification of motor unit spike trains from high-density surface EMG," *IEEE Trans. Neural Syst. Rehabil. Eng.*, vol. 18, no. 3, pp. 221–229, Jun. 2010.

[3] X. Li, Y.-C. Wang, N. L. Suresh, W. Z. Rymer, and P. Zhou, "Motor unit number reductions in paretic muscles of stroke survivors," *IEEE Trans. Inf. Technol. Biomed.*, vol. 15, no. 4, pp. 505–512, Jul. 2011.

[4] E. Scheme and K. Englehart, "Electromyogram pattern recognition for control of powered upper-limb prostheses: State of the art and challenges for clinical use," *J. Rehabil. Res. Develop.*, vol. 48, no. 6, p. 643, 2011.

[5] K. Englehart, B. Hudgins, and P. A. Parker, "A wavelet-based continuous classification scheme for multifunction myoelectric control," *IEEE Trans. Biomed. Eng.*, vol. 48, no. 3, pp. 302–311, Mar. 2001.

[6] M. A. Oskoei and H. Hu, "Myoelectric control systems—A survey," *Biomed. Signal Process. Control*, vol. 2, no. 4, pp. 275–294, 2007.

[7] A. E. Schultz and T. A. Kuiken, "Neural interfaces for control of upper limb prostheses: The state of the art and future possibilities," *PM R*, vol. 3, no. 1, pp. 55–67, 2011.

[8] F. J. Valero-Cuevas, F. E. Zajac, and C. G. Burgar, "Large index-fingertip forces are produced by subject-independent patterns of muscle excitation," *J. Biomech.*, vol. 31, no. 8, pp. 693–703, 1998.

[9] G. Torres-Oviedo and L. H. Ting, "Subject-specific muscle synergies in human balance control are consistent across different biomechanical contexts," *J. Neurophys.*, vol. 103, no. 6, pp. 3084–3098, 2010.

[10] V. T. Inman, H. J. Ralston, J. R. De C. M. Saunders, M. B. B. Feinstein, and E. W. Wright, Jr., "Relation of human electromyogram to muscular tension," *Electroencephalogr. Clin. Neurophysiol.*, vol. 4, no. 2, pp. 187–194, 1952.

[11] O. C. J. Lippold, "The relation between integrated action potentials in a human muscle and its isometric tension," *J. Physiol.*, vol. 117, no. 4, pp. 492–499, 1952.

[12] H. S. Milner-Brown and R. B. Stein, "The relation between the surface electromyogram and muscular force," *J. Physiol.*, vol. 246, no. 3, pp. 549–569, Apr. 1975.

[13] A. A. Biewener, J. M. Wakeling, S. S. Lee, and A. S. Arnold, "Validation of hill-type muscle models in relation to neuromuscular recruitment and force–velocity properties: Predicting patterns of *in vivo* muscle force," *Integr. Comparative Biol.*, vol. 54, no. 6, pp. 1072–1083, 2014.

[14] J. M. Wakeling, S. S. Lee, A. S. Arnold, M. de Boef Miara, and A. A. Biewener, "A muscle's force depends on the recruitment patterns of its fibers," *Ann. Biomed. Eng.*, vol. 40, no. 8, pp. 1708–1720, 2012.

[15] E. J. Perreault, C. J. Heckman, and T. G. Sandercock, "Hill muscle model errors during movement are greatest within the physiologically relevant range of motor unit firing rates," *J. Biomech.*, vol. 36, no. 2, pp. 211–218, 2003.

[16] W. F. Genadry, R. E. Kearney, and I. W. Hunter, "Dynamic relationship between EMG and torque at the human ankle: Variation with contraction level and modulation," *Med. Biol. Eng. Comput.*, vol. 26, no. 5, pp. 489–496, 1988.

[17] G. L. Gottlieb and G. C. Agarwal, "Dynamic relationship between isometric muscle tension and the electromyogram in man," *J. Appl. Physiol.*, vol. 30, no. 3, pp. 345–351, 1971.

[18] J. C. Coggshall and G. A. Bekey, "EMG-force dynamics in human skeletal muscle," *Med. Biol. Eng.*, vol. 8, no. 3, pp. 265–270, 1970.

[19] P. A. Crosby, "Use of surface electromyogram as a measure of dynamic force in human limb muscles," *Med. Biol. Eng. Comput.*, vol. 16, no. 5, pp. 519–524, 1978.

[20] A. C. Schouten, E. De Vlugt, J. J. Van Hilten, and F. C. T. Van Der Helm, "Quantifying proprioceptive reflexes during position control of the human arm," *IEEE Trans. Biomed. Eng.*, vol. 55, no. 1, pp. 311–321, Jan. 2008.

[21] T. Sinkjær, E. Toft, K. Larsen, and S. Andreassen, "EMG-torque dynamics at different contraction levels in human ankle muscles," *J. Electromyogr. Kinesiol.*, vol. 3, no. 2, pp. 67–77, 1993.

[22] J. Soechting and W. J. Roberts, "Transfer characteristics between EMG activity and muscle tension under isometric conditions in man," *J. Physiol.*, vol. 70, no. 6, pp. 779–793, 1976.

[23] E. A. Clancy, O. Bida, and D. Rancourt, "Influence of advanced electromyogram (EMG) amplitude processors on EMG-to-torque estimation during constant-posture, force-varying contractions," *J. Biomech.*, vol. 39, no. 14, pp. 2690–2698, 2006.

[24] E. N. Kamavuako, E. J. Scheme, and K. B. Englehart, "Wrist torque estimation during simultaneous and continuously changing movements: Surface vs. untargeted intramuscular EMG," *J. Neurophysiol.*, vol. 109, no. 11, pp. 2658–2665, 2013.

[25] A. C. S. Schouten, E. De Vlugt, and F. C. T. Van Der Helm, "Design of perturbation signals for the estimation of proprioceptive reflexes," *IEEE Trans. Biomed. Eng.*, vol. 55, no. 5, pp. 1612–1619, May 2008.

[26] A. C. Schouten, W. Mugge, and F. C. van der Helm, "NMClab, a model to assess the contributions of muscle visco-elasticity and afferent feedback to joint dynamics," *J. Biomech.*, vol. 41, no. 8, pp. 1659–1667, 2008.
[27] M. A. Golkar and R. E. Kearney, "Closed-loop identification of the dynamic relation between surface EMG and torque at the human ankle," *IFAC-PapersOnLine*, vol. 48, no. 28, pp. 263–268, 2015.
[28] R. L. Morier, P. L. Weiss, and R. E. Kearney, "Low inertia, rigid limb fixation using glass fibre casting bandage," *Med. Biol. Eng. Comput.*, vol. 28, no. 1, pp. 96–99, 1990. [Online]. Available: http://dx.doi.org/10.1007/BF02441686
[29] B. Freriks and H. Hermens, "European recommendations for surface electromyography," *Roessingh Res. Develop.*, vol. 8, no. 2, pp. 13–54, 2000.
[30] C. J. De Luca, L. D. Gilmore, M. Kuznetsov, and S. H. Roy, "Filtering the surface EMG signal: Movement artifact and baseline noise contamination," *J. Biomech.*, vol. 43, no. 8, pp. 1573–1579, 2010.
[31] S. Day, "Important factors in surface EMG measurement," Bortec Biomed. Ltd, Calgary, AB, Canada, Tech. Rep., 2002, pp. 1–17.
[32] R. Pintelon and J. Schoukens, *System Identification: A Frequency Domain Approach*. Hoboken, NJ, USA: Wiley, 2012.
[33] D. T. Westwick and R. E. Kearney, *Identification of Nonlinear Physiological Systems*, vol. 7. Hoboken, NJ, USA: Wiley, 2003.
[34] D. T. Westwick and E. J. Perreault, "Closed-loop identification: Application to the estimation of limb impedance in a compliant environment," *IEEE Trans. Biomed. Eng.*, vol. 58, no. 3, pp. 521–530, Mar. 2011.
[35] P. E. Caines, *Linear Stochastic Systems*. Hoboken, NJ, USA: Wiley, 1987.
[36] C.-Y. Dong, T.-W. Yoon, D. G. Bates, and K.-H. Cho, "Identification of feedback loops embedded in cellular circuits by investigating non-causal impulse response components," *J. Math. Biol.*, vol. 60, no. 2, pp. 285–312, 2010.
[37] J. Houk and E. Henneman, "Responses of Golgi tendon organs to active contractions of the soleus muscle of the cat," *J. Neurophysiol.*, vol. 30, no. 3, pp. 466–481, 1967.
[38] J. K. S. Jansen and T. Rudjord, "On the silent period and Golgi tendon organs of the soleus muscle of the cat," *Acta Physiol. Scandin.*, vol. 62, no. 4, pp. 364–379, 1964.
[39] M. P. Mileusnic and G. E. Loeb, "Mathematical models of proprioceptors. II. Structure and function of the Golgi tendon organ," *J. Neurophysiol.*, vol. 96, no. 4, pp. 1789–1802, 2006.
[40] M. D. Binder, J. S. Kroin, G. P. Moore, and D. G. Stuart, "The response of Golgi tendon organs to single motor unit contractions," *J. Physiol.*, vol. 271, no. 2, pp. 337–349, 1977.
[41] L. Jami, "Golgi tendon organs in mammalian skeletal muscle: Functional properties and central actions," *Physiol. Rev.*, vol. 72, no. 3, pp. 623–666, 1992.
[42] B. H. C. Matthews, "Nerve endings in mammalian muscle," *J. Physiol.*, vol. 78, no. 1, pp. 1–53, 1933.
[43] C. Ghez, J. Gordon, and M. F. Ghilardi, "Impairments of reaching movements in patients without proprioception. II. Effects of visual information on accuracy," *J. Neurophysiol.*, vol. 73, no. 1, pp. 361–372, Jan. 1995.
[44] E. R. Kandel, J. H. Schwartz, and T. M. Jessell, *Principles of Neural Science*, vol. 4. New York, NY, USA: McGraw-Hill, 2000.
[45] J. E. Desmedt and E. Godaux, "Ballistic contractions in man: Characteristic recruitment pattern of single motor units of the tibialis anterior muscle," *J. Physiol.*, vol. 264, no. 3, pp. 673–693, 1977.
[46] M. Kawato, "Internal models for motor control and trajectory planning," *Current Opinion Neurobiol.*, vol. 9, no. 6, pp. 718–727, 1999.
[47] S. Erimaki, O. M. Agapaki, and C. N. Christakos, "Neuromuscular mechanisms and neural strategies in the control of time-varying muscle contractions," *J. Neurophysiol.*, vol. 110, no. 6, pp. 1404–1414, 2013.
[48] R. Plamondon and A. M. Alimi, "Speed/accuracy trade-offs in target-directed movements," *Behav. Brain Sci.*, vol. 20, no. 2, pp. 279–303, 1997.
[49] M. Desmurget and S. Grafton, "Forward modeling allows feedback control for fast reaching movements," *Trends Cognit. Sci.*, vol. 4, no. 11, pp. 423–431, 2000.
[50] D. A. McCrea, "Spinal circuitry of sensorimotor control of locomotion," *J. Physiol.*, vol. 533, no. 1, pp. 41–50, 2001.
[51] R. B. Stein and C. Capaday, "The modulation of human reflexes during functional motor tasks," *Trends Neurosci.*, vol. 11, no. 7, pp. 328–332, 1988.
[52] J. D. Brooke, J. Cheng, D. F. Collins, W. E. McIlroy, J. E. Misiaszek, and W. R. Staines, "Sensori-sensory afferent conditioning with leg movement: Gain control in spinal reflex and ascending paths," *Progr. Neurobiol.*, vol. 51, no. 4, pp. 393–421, 1997.
[53] R. Xia, B. M. Bush, and G. M. Karst, "Phase-dependent and task-dependent modulation of stretch reflexes during rhythmical hand tasks in humans," *J. Physiol.*, vol. 564, no. 3, pp. 941–951, 2005.
[54] M. A. Golkar and R. E. Kearney, "Effects of input frequency content and signal-to-noise ratio on the parametric estimation of surface EMG-Torque dynamics," in *Proc. IEEE 38th Annu. Int. Conf. Eng. Med. Biol. Soc. (EMBC)*, Aug. 2016, pp. 1712–1716.
[55] J. E. Desmedt and E. Godaux, "Voluntary motor commands in human ballistic movements," *Ann. Neurol.*, vol. 5, no. 5, pp. 415–421, 1979.
[56] E. A. Clancy, S. Bouchard, and D. Rancourt, "Estimation and application of EMG amplitude during dynamic contractions," *IEEE Eng. Med. Biol. Mag.*, vol. 20, no. 6, pp. 47–54, Nov. 2001.
[57] E. Park and S. G. Meek, "Adaptive filtering of the electromyographic signal for prosthetic control and force estimation," *IEEE Trans. Biomed. Eng.*, vol. 42, no. 10, pp. 1048–1052, Oct. 1995.
[58] E. A. Clancy, "Electromyogram amplitude estimation with adaptive smoothing window length," *IEEE Trans. Biomed. Eng.*, vol. 46, no. 6, pp. 717–729, Jun. 1999.
[59] T. D'Alessio, "Analysis of a digital EMG signal processor in dynamic conditions," *IEEE Trans. Biomed. Eng.*, vol. BME-32, no. 1, pp. 78–82, Jan. 1985.
[60] Y. St-Amant, D. Rancourt, and E. A. Clancy, "Influence of smoothing window length on electromyogram amplitude estimates," *IEEE Trans. Biomed. Eng.*, vol. 45, no. 6, pp. 795–799, Jun. 1998.
[61] O. Mohamed, J. Perry, and H. Hislop, "Relationship between wire EMG activity, muscle length, and torque of the hamstrings," *Clin. Biomech.*, vol. 17, no. 8, pp. 569–579, 2002.
[62] P. Liu, L. Liu, F. Martel, D. Rancourt, and E. A. Clancy, "Influence of joint angle on EMG–torque model during constant-posture, quasi-constant-torque contractions," *J. Electromyogr. Kinesiol.*, vol. 23, no. 5, pp. 1020–1028, 2013.